JCI The Journal of Clinical Investigation

Androgen deprivation–induced NCoA2 promotes metastatic and castration-resistant prostate cancer

Jun Qin, … , Sophia Y. Tsai, Ming-Jer Tsai

J Clin Invest. 2014;124(11):5013-5026. https://doi.org/10.1172/JCI76412.

Research Article **Oncology**

A major clinical hurdle for the management of advanced prostate cancer (PCa) in patients is the resistance of tumors to androgen deprivation therapy (ADT) and their subsequent development into castration-resistant prostate cancer (CRPC). While recent studies have identified potential pathways involved in CRPC development, the drivers of CRPC remain largely undefined. Here we determined that nuclear receptor coactivator 2 (NCoA2, also known as SRC-2), which is frequently amplified or overexpressed in patients with metastatic PCa, mediates development of CRPC. In a murine model, overexpression of NCoA2 in the prostate epithelium resulted in neoplasia and, in combination with *Pten* deletion, promoted the development of metastasis-prone cancer. Moreover, depletion of NCoA2 in PTEN-deficient mice prevented the development of CRPC. In human androgen-sensitive prostate cancer cells, androgen signaling suppressed NCoA2 expression, and NCoA2 overexpression in murine prostate tumors resulted in hyperactivation of PI3K/AKT and MAPK signaling, promoting tumor malignance. Analysis of PCa patient samples revealed a strong correlation among NCoA2-mediated signaling, disease progression, and PCa recurrence. Taken together, our findings indicate that androgen deprivation induces NCoA2, which in turn mediates activation of PI3K signaling and promotes PCa metastasis and CRPC development. Moreover, these results suggest that the inhibition of NCoA2 has potential for PCa therapy.

Androgen deprivation–induced NCoA2 promotes metastatic and castration-resistant prostate cancer

Jun Qin,[1,2] Hui-Ju Lee,[2] San-Pin Wu,[2,3] Shih-Chieh Lin,[2] Rainer B. Lanz,[2] Chad J. Creighton,[4] Francesco J. DeMayo,[2,4] Sophia Y. Tsai,[2,4,5] and Ming-Jer Tsai[2,4,5]

[1]Institute of Health Sciences, Shanghai Institutes for Biological Sciences, Chinese Academy of Sciences and Shanghai JiaoTong University School of Medicine, Shanghai, China. [2]Department of Molecular and Cellular Biology, Baylor College of Medicine, Houston, Texas, USA. [3]Adrienne Helis Malvin Medical Research Foundation, New Orleans, Louisiana, USA. [4]Dan L. Duncan Cancer Center and [5]Program in Developmental Biology, Baylor College of Medicine, Houston, Texas, USA.

A major clinical hurdle for the management of advanced prostate cancer (PCa) in patients is the resistance of tumors to androgen deprivation therapy (ADT) and their subsequent development into castration-resistant prostate cancer (CRPC). While recent studies have identified potential pathways involved in CRPC development, the drivers of CRPC remain largely undefined. Here we determined that nuclear receptor coactivator 2 (NCoA2, also known as SRC-2), which is frequently amplified or overexpressed in patients with metastatic PCa, mediates development of CRPC. In a murine model, overexpression of NCoA2 in the prostate epithelium resulted in neoplasia and, in combination with *Pten* deletion, promoted the development of metastasis-prone cancer. Moreover, depletion of NCoA2 in PTEN-deficient mice prevented the development of CRPC. In human androgen-sensitive prostate cancer cells, androgen signaling suppressed NCoA2 expression, and NCoA2 overexpression in murine prostate tumors resulted in hyperactivation of PI3K/AKT and MAPK signaling, promoting tumor malignance. Analysis of PCa patient samples revealed a strong correlation among NCoA2-mediated signaling, disease progression, and PCa recurrence. Taken together, our findings indicate that androgen deprivation induces NCoA2, which in turn mediates activation of PI3K signaling and promotes PCa metastasis and CRPC development. Moreover, these results suggest that the inhibition of NCoA2 has potential for PCa therapy.

Introduction

Prostate cancer (PCa), the second most common cancer diagnosed in men worldwide (1), proceeds through a series of defined states, classified as prostatic intraepithelial neoplasia (PIN), PCa in situ, and invasive and metastatic cancer (2). Various molecular events including phosphatase and tensin homolog (*PTEN*) mutation, TMPRSS2-ERG translocation, NKX3.1 downregulation, and Myc upregulation are observed in a large percentage of prostate carcinomas and have been implicated in playing critical roles in prostate tumorigenesis and the development of castration-resistant PCa (CRPC) (3–9).

PTEN loss or PI3K/AKT signaling pathway activation tightly correlates with human PCa progression and metastasis. Up to 70% of metastatic PCa exhibits loss of PTEN function or genomic alterations in the PI3K signaling pathway (3, 9, 10); this places *PTEN* mutations among the most common genetic alterations reported in PCa. Genetic studies in mice have been crucial in understanding the role of PTEN/PI3K signaling in tumorigenesis. Conditional prostate-specific *Pten* deletion in mice showed that PTEN-null PCa progresses with defined kinetics that mimics histopathological features of the human disease (3, 11). However, tumors bearing PTEN alternations in mice can progress to adenocarcinoma, but they rarely develop into invasive carcinoma. Therefore, PTEN-null mice provide an excellent model for identifying the pathway or players that could serve as the "second hit" to drive the indolent tumors to acquire full penetrance of metastatic potential. Recent studies indicate that loss of PTEN triggers a defense mechanism to activate TGF-β signaling (12, 13), while overexpression of COUP-TFII disrupts the TGF-β–dependent growth barrier to promote tumor metastasis (13). These results suggest that feedback pathways suppressing progression might be activated in indolent tumors, and inhibition of such barriers to progression would lead to the development of metastasis-prone cancer. In support of this notion, AKT phosphatase PH domain and leucine rich repeat protein phosphatase 1 and 2 (PHLPP1/2) also exert a surveillance function to form a common barrier against PCa progression (14). Inactivation of PHLPP1 and PTEN triggers a growth-suppressive response via an increase in p53 and PHLPP2. In patients, co-deletion of *PTEN* and *PHLPP1* is highly restricted to metastatic disease and tightly correlated with the deletion of *P53* and *PHLPP2* (14). Thus, it is critical to dissect the underlying mechanism that promotes PTEN-mutant tumors to develop into metastasis-prone cancer. Understanding such a mechanism would likely benefit PCa disease diagnosis and intervention.

Although androgen deprivation is the most commonly employed therapeutic treatment for PCa, the majority of patients subsequently succumb to castration-resistant disease (15). Notably, even when PCa progresses to castration resistance, androgen receptor (AR) activation and signaling still remain sustained through a variety of mechanisms, including amplification of

Authorship note: Jun Qin and Hui-Ju Lee contributed equally to this work.
Conflict of interest: The authors have declared that no conflict of interest exists.
Submitted: April 1, 2014; **Accepted:** September 4, 2014.
Reference information: *J Clin Invest*. 2014;124(11):5013–5026. doi:10.1172/JCI76412.

the *AR* gene, gain-of-function mutations of *AR* that may confer increased protein stability, sensitivity to androgens, novel responses to other steroid hormones, ligand-independent activity, or increased recruitment of AR coactivator proteins (2, 15, 16). Intriguingly, recent studies indicate that reciprocal feedback inhibition of PI3K and AR signaling also plays a critical role in the development of CRPC (17, 18). Androgen deprivation therapy (ADT) stimulates AKT signaling to sustain the growth of PCa cells partly through downregulation of FKBP5 expression. In addition, compelling evidence suggests that MAPK pathway activation also plays a significant role in human PCa progression, particularly in metastasis and CRPC development (19, 20). Thus, the signaling circuits involved in CRPC are tightly orchestrated.

Nuclear receptor coactivator 2 (NCoA2; also known as SRC-2, TIP2, or GRIP1), a member of the p160 family of transcriptional coregulators, does not bind DNA directly but is recruited to the enhancer or promoter regions of target genes through interaction with transcription factors to modulate transcription (21–24). NCoA2 plays a variety of roles in different physiological processes, including cellular growth, energy metabolism, circadian rhythm, feeding behavior, and heart function (21–25). In patients with PCa, NCoA2 is frequently amplified or overexpressed in 8% of the primary tumors; the frequency is even higher at 37% in patients with metastatic cancer (9). More importantly, patients bearing higher levels of NCoA2 are more likely to relapse after ADT (26). In the present study, we utilized genetically engineered mouse models (GEMs) together with patient specimen analysis to define the role of NCoA2 in metastatic and CRPC, and dissect the mechanism by which NCoA2 contributes to prostate tumorigenesis.

Results

NCoA2 is sufficient to initiate epithelial neoplastic transformation. Consistent with a recent report (9), results from public dataset mining and Oncomine expression analysis indicated that *NCOA2* expression was significantly upregulated in metastatic PCa patients (Supplemental Figure 1; supplemental material available online with this article; doi:10.1172/JCI76412DS1). Thus, we sought to generate NCoA2 transgenic mice resembling NCoA2 overexpression in patients, to define whether NCoA2 plays a causal role in PCa. To this end, we generated mice that can overexpress NCoA2 in a tissue-specific manner ($NCoA2^{OE/+}$), which harbor a single copy of a mini-gene consisting of a hybrid chicken β-actin and cytomegalovirus (CAGGS) promoter, a loxP-STOP-loxP (LSL) cassette (a stop cassette consisting of 4 copies of SV40 polyadenylation sequences), and *Ncoa2* cDNA (Figure 1A). As expected, $NCoA2^{OE/+}$ mice were generally healthy without obvious defects in growth and reproduction. Upon crossing these mice with probasin-*Cre* ($PB^{CRE/+}$) mice (27), Cre recombinase–mediated activation removed the LSL stop cassette, allowing the CAGGS promoter to drive the constitutive expression of *Ncoa2*. Overexpression of NCoA2 was thus achieved exclusively within the prostate epithelium (hereafter referred as $NCoA2^{PCOE/+}$ mice) in a temporal- and spatial-specific manner (Figure 1B). First, we aimed to define whether this $NCoA2^{PCOE/+}$ mouse model could reflect the pathological conditions in PCa. Thus, we compared the abundance of *Ncoa2* mRNA or protein in our mouse model with that in human PCa cell lines as well as in castrated mice (Figure 1, C and D). The results clearly indicated that the degree of overexpression in our mouse model was comparable with the levels observed in PCa cell lines and castrated mice, suggesting that the $NCoA2^{PCOE/+}$ mice utilized in this study largely reflected the pathological conditions in human PCa.

Over the course of more than 1 year, we observed that the $NCoA2^{PCOE/+}$ mice frequently displayed prostate epithelial hyperplasia and dysplasia and often developed low-grade PIN (LGPIN). Histopathological analyses of all 3 lobes of the prostate revealed that 60% of $NCoA2^{PCOE/+}$ animals developed hyperplasia or multifocal PIN lesions at 14 months of age. While NCoA2 overexpression alone was sufficient to mimic early stages of human PCa in mice, it did not develop adenocarcinoma for over 16 months. As shown in Figure 1E, $NCoA2^{PCOE/+}$ PINs displayed micropapillary, cribriform, and/or tuft-like structural organizations reminiscent of human PINs, whereas control mice displayed normal prostatic histology. Taken together, these results demonstrate that NCoA2 overexpression is sufficient to initiate epithelial neoplastic transformation, corroborating a notion that *NCOA2* is an oncogene for PCa.

NCoA2 collaborates with PTEN loss to promote PCa progression and metastasis. The absence of adenocarcinoma in $NCoA2^{PCOE/+}$ prostates prompted us to investigate whether additional mutations could collaborate with NCoA2 overexpression to promote prostate tumorigenesis. *PTEN* is frequently mutated in PCa patients, and prostate-specific *Pten* deletion mice represent an excellent mouse model in which tumor progression mimics histopathologic features of the human disease (3). Since partially reduced PTEN expression occurs frequently during human PCa progression (9), we crossed $NCoA2^{OE/+}$ mice with *Pten* floxed mice (3) and then with probasin-*Cre* mice, to generate prostatic NCoA2 overexpression in a PTEN heterozygous background (probasin-*Cre* $Pten^{fl/+}$ $NCoA2^{OE/+}$ mice, hereafter referred to as $PTEN^{PC+/-}$ $NCoA2^{PCOE/+}$ mice). Though *Pten* heterozygous mice develop PIN after a long latency with incomplete penetrance (3), prostate-specific overexpression of NCoA2 in a *Pten* heterozygous background resulted in a rapid acceleration of tumor progression, with overt and high penetrance of high-grade PIN (HGPIN) starting at 6–7 months of age and progressing to invasive adenocarcinoma by 12 months (Figure 2A and Supplemental Figure 2). At about 7 months of age, tumors bearing NCoA2 overexpression had advanced to HGPIN or adenocarcinoma, whereas $PTEN^{PC+/-}$ mice showed normal prostatic histology or hyperplasia (Supplemental Figure 2, A and B). Accordingly, $PTEN^{PC+/-}$ $NCoA2^{PCOE/+}$ compound mice displayed a higher proliferative index as seen by an increase in numbers of Ki67-positive cells in comparison with $PTEN^{PC+/-}$ mice, whereas cellular apoptosis remained the same between $PTEN^{PC+/-}$ and $PTEN^{PC+/-}$ $NCoA2^{PCOE/+}$ mice (Figure 2B).

To better visualize tumor progression and metastasis in vivo, we also crossed these compound mice with Rosa26-LSL-luciferase reporter mice (28) for imaging analysis of luminescent signals. Consistent with H&E staining and macroscopic dissection image as indicated in Figure 1E and Figure 2C, we observed that the luminescence intensity of $NCoA2^{PCOE/+}$ mice was slightly higher than that in control mice (Supplemental Figure 2C). In addition, $PTEN^{PC+/-}NCoA2^{PCOE/+}$ mice displayed stronger luciferase intensities

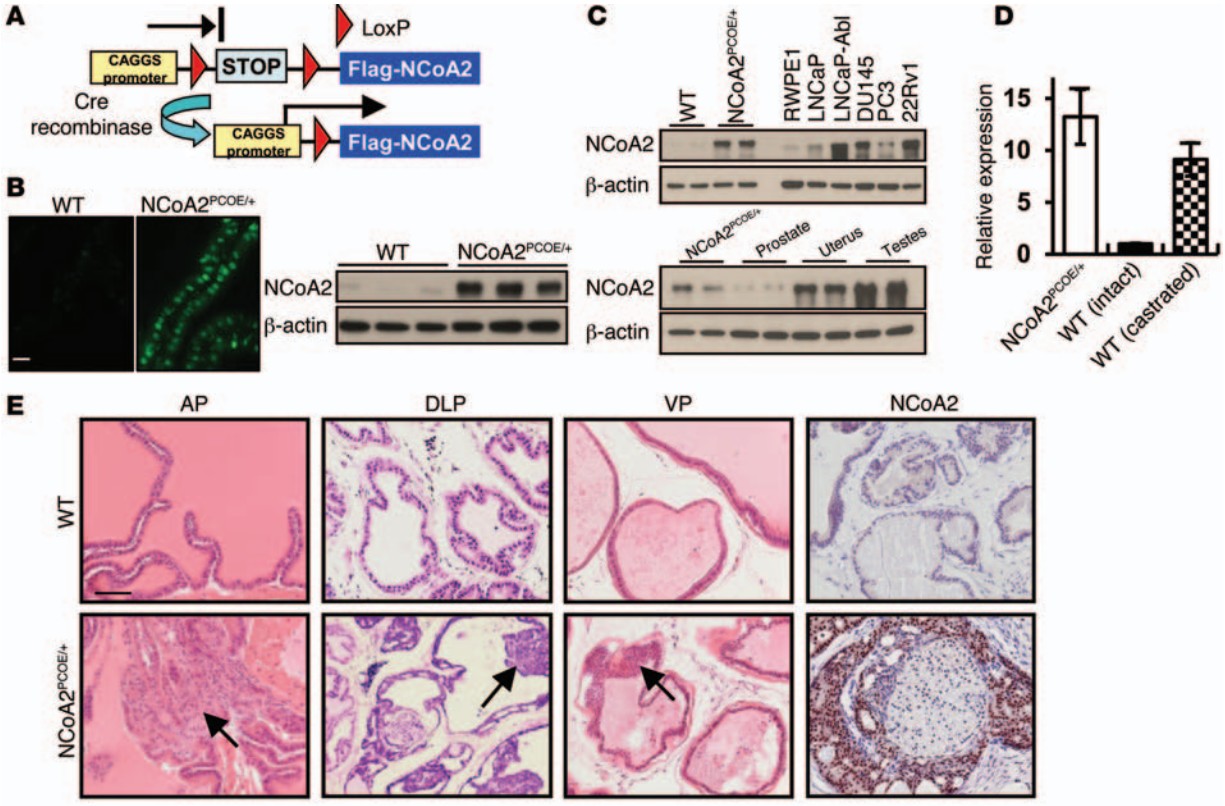

Figure 1. Oncogenic role of NCoA2 in PIN. (**A**) Scheme of conditional overexpression of NCoA2 (ROSA26 Lox-STOP-Lox; Flag-*NCoA2*$^{OE/+}$). (**B**) IF and Western blot analysis of NCoA2 overexpression in prostate epithelium from wild-type and NCoA2$^{PCOE/+}$ mice at 2 months of age. (**C**) Top: Western blot analysis of NCoA2 expression in the prostates from wild-type and NCoA2$^{PCOE/+}$ mice, immortalized prostate epithelial cells, RWPE1, and prostate cancer cells including LNCaP, LNCaP-Abl, DU145, PC3, and 22Rv1. Bottom: NCoA2 expression in NCoA2$^{PCOE/+}$ and wild-type mice. (**D**) qRT-PCR analysis of *Ncoa2* expression in the prostates from NCoA2$^{PCOE/+}$ mice and the intact or castrated wild-type mice. (**E**) H&E-stained sections of representative anterior prostate (AP), dorsolateral prostate (DLP), and ventral prostate (VP) at 14 months of age in wild-type and NCoA2$^{PCOE/+}$ mice. Arrows indicate PIN (bottom). Scale bars: 20 μm (**B**); 50 μm (**E**).

in the primary prostate sites than did PTEN$^{PC+/-}$ mice (Figure 2C). These results are consistent with the notion that NCoA2 overexpression causes neoplasia and, on partial loss of PTEN, carcinoma in the mouse prostate.

It is generally believed that *PTEN*-mutant tumors are indolent, in which tumor cells are well confined within layers of α-SMA–positive smooth muscle cells. Interestingly, we found that the smooth muscle sheaths surrounding the tumors in NCoA2-overexpressing mice were disrupted and/or partially lost (Figure 2D). As a consequence, tumor cells were seen to invade into the stromal compartment as indicated by CK8 and AR immunostaining (Figure 2D and Supplemental Figure 2D), suggesting that tumor cells bearing high levels of NCoA2 are more invasive. In agreement with the invasive phenotype observed in the primary sites, PCa-bearing PTEN$^{PC+/-}$ NCoA2$^{PCOE/+}$ mice showed a metastatic spread of AR or CK8-positive tumor nodules to the draining lumbar lymph nodes in 9/14 cases and to the lungs in 5/14 cases (Figure 2E and Table 1). This result was further supported by observations using luciferase reporter mice and quantitative RT-PCR (qRT-PCR) analysis of prostatic-specific gene expression (*Ar* and *Ck8*), which demonstrated metastatic spreading of tumor cells in the distant organs upon NCoA2 overexpression at 1 year of age (Figure 2, C and E, and Supplemental Figure 2E). In sharp contrast, PTEN$^{PC+/-}$ mice did not develop lung metastatic lesions, and less than 20% of mice showed lymph node metastasis at 1 year of age (Figure 2E and Table 1). Collectively, NCoA2 collaborates with PTEN loss to produce the full spectrum of PCa phenotypes, leading to metastatic disease in *Pten* heterozygous mutants.

NCoA2 expression is suppressed by androgen signaling. Having established the role of NCoA2 in prostate tumorigenesis, we attempted to address which signals stimulate NCoA2 expression in PCa. It has been shown that NCoA2 expression is suppressed by androgen signaling in cultured cells (26). Thus, we examined whether androgen deprivation could indeed enhance NCoA2 expression in the wild-type prostate and PTEN-null prostate tumors. As shown in Figure 3A, castration significantly stimulated the expression of NCoA2 in a PTEN-independent manner. In addition, depletion of AR or supplement of AR agonist R1881 resulted in enhanced or reduced expression of NCoA2 in LNCaP cells, respectively (Supplemental Figure 3A). Furthermore, ChIP–quantitative PCR (ChIP-qPCR) analyses indicated that AR was directly recruited to the NCoA2 proximal promoter and presumably inhibited *Ncoa2* transcription (Supplemental Figure 3B). In support of this finding, depletion of AR by RNAi in LNCaP cells profoundly enhanced the luciferase activity driven by the *Ncoa2* promoter, whereas mutation of the putative AR binding site in the *Ncoa2* promoter abolished this stimulation (Supplemental Figure 3C). Taken together, these findings indi-

Table 1. Metastatic incidence between PTEN$^{PC+/-}$ and PTEN$^{PC+/-}$ NCoA2$^{PCOE/+}$ mice

Location	PTEN$^{PC+/-}$ (*n*)	PTEN$^{PC+/-}$ NCoA2$^{PCOE/+}$ (*n*)	*P*
Lymph node	2/12	9/14	0.0123
Lung	0/12	5/14	0.0425

Summary of metastatic incidence between PTEN$^{PC+/-}$ and PTEN$^{PC+/-}$ NCoA2$^{PCOE/+}$ mice at 12 months of age. Fisher exact test (2-tailed) was used for statistical analysis.

cate that AR serves as an upstream regulator to transcriptionally inhibit NCoA2 expression in PCa cells.

NCoA2 elevation, as induced by androgen deprivation, causes CRPC. Given the fact that patients bearing higher levels of NCoA2 are more likely to relapse after androgen ablation (26), we postulated that upregulation of NCoA2 upon androgen deprivation may compensate for the decrease of AR activity to cause the development of CRPC. In support of this notion, we observed that depletion of NCoA2 reduced androgen-independent growth of LNCaP-Abl cells (Figure 3B). Conversely, overexpression of NCoA2 in androgen-dependent LNCaP cells rendered the cells to become more resistant to androgen deprivation (Supplemental Figure 4A). Encouraged by these cell culture results, we utilized genetic mouse models to determine whether NCoA2 leads tumor cells to become resistant to androgen deprivation. Given that PTEN signaling is implicated in the development of CRPC (17, 18), we took advantage of castrated *Pten*-null mice (high NCoA2) to examine whether ablation of NCoA2 will compromise the development of CRPC. To this end, we generated an array of mouse models, including probasin-*Cre Pten$^{fl/fl}$* mice (prostate-specific PTEN-null; referred to herein as PTEN$^{PC-/-}$) and probasin-*Cre Ncoa2$^{fl/fl}$* mice (prostate-specific NCoA2-null; PTEN$^{PC-/-}$ NCoA2$^{PC-/-}$) without or with castration that elicits NCoA2 overexpression (Supplemental Figure 4B). For each genetically distinct tumor type, we generated cohorts of more than 8 mutant mice that were castrated at the age of 4 months old, a time at which the mice have already developed HGPIN. Age-matched, non-castrated cohorts were used as controls. All cohorts were monitored for a 6-month period after castration.

In agreement with previous reports (17, 18), we observed that androgen-independent proliferation was intrinsic to PTEN loss, independent of androgen signaling (Figure 3C and Supplemental Figure 4C). However, cell death index was increased in PTEN-null mice upon castration (Supplemental Figure 4D). Over time, androgen-independent growth overrides androgen-dependent death and produces castration-resistant growth and invasive adenocarcinoma. Importantly, we found that inactivation of NCoA2 in castrated PTEN$^{PC-/-}$ mice profoundly compromised cell proliferation (Figure 3C and Supplemental Figure 4C), suggesting that NCoA2 is critical for PTEN mutant tumors to acquire androgen-independent growth. Further pathological examination of dorsolateral prostate lobes from 6-month-old castrated PTEN-null mice displayed a clear development of invasive cancer, as evidenced by H&E staining (Figure 3D) and loss or discontinuous staining of α-SMA (Figure 3F). Moreover, subsets of invasive tumor cells in castrated PTEN-null mice were found to undergo epithelial-mesenchymal transition, as reflected by reduced E-cadherin expression and co-expression of the mesenchymal marker vimentin (Figure 3, G and H). Notably, CK8 positivity of the invading tumors indicated their epithelial origin (Supplemental Figure 4E). In sharp contrast to this finding, ablation of NCoA2 largely diminished the production of invasive tumors and profoundly arrested tumor progression at the LGPIN stages (Figure 3, D–H). The quantitative results are summarized in Figure 3E and clearly indicated that castration promoted PTEN-null tumors to develop into invasive cancer, whereas ablation of NCoA2 prevented such development and arrested tumors at the LGPIN stages. In accordance with these results, metastatic spread of CK8-positive tumor nodules to lumbar lymph nodes, the majority of which were also AR positive, were concomitantly reduced in castrated PTEN$^{PC-/-}$ NCoA2$^{PC-/-}$ mice (Figure 3I and Supplemental Figure 4F). All these results indicate that NCoA2 enables the castrated PTEN-null mice to acquire the onset of CRPC. Notably, given that NCoA2 expression is very low in non-castrated wild-type and PTEN$^{PC-/-}$ mice, it is not surprising that intact NCoA2$^{PC-/-}$ and PTEN$^{PC-/-}$ NCoA2$^{PC-/-}$ mice lacked a discernible phenotype. As indicated in Supplemental Figure 5, NCoA2$^{PC-/-}$ mice displayed normal prostatic histology when monitored for more than 1 year. In addition, both PTEN$^{PC-/-}$ and PTEN$^{PC-/-}$ NCoA2$^{PC-/-}$ intact mice developed HGPIN or invasive cancer with a similar incidence (Figure 3, D–I). Taken together, these results establish a causal role of NCoA2 in the development of CRPC upon androgen deprivation.

NCoA2 activates PI3K/AKT and MAPK signaling in PCa. To dissect the underlying mechanism for how NCoA2 promotes prostate tumorigenesis, we conducted transcriptome comparison of PTEN$^{PC+/-}$ and PTEN$^{PC+/-}$ NCoA2$^{PCOE/+}$ prostates to gain genomic insights into the biological processes affected by NCoA2 overexpression. Unbiased gene ontology analysis revealed that the most prominent altered gene categories in NCoA2-overexpressing cells were associated with functional annotation referred to as "molecular mechanism of various cancer" and "MAPK signaling" (Supplemental Figure 6). To gain further molecular insights into how NCoA2 influences PCa, we performed pathway enrichment analysis (29) within the NCoA2-regulated gene signature. Consistent with the oncogenic roles of NCoA2 observed in mouse models, transcriptomic signature assays indicated that many signaling pathways that play critical roles in prostate tumorigenesis were altered upon NCoA2 overexpression. As shown in Figure 4A and Supplemental Table 2, there was significant enrichment of *PTEN* loss, *AKT* activation, *MAPK*, *MEK*, and *EGFR* signatures among NCoA2-regulated genes, which suggests that NCoA2 might exert its function through modulating these multiple pathways during prostate tumorigenesis.

Of note, PTEN, PI3K/AKT, and MAPK signaling pathways have all been shown to be critical for prostate tumorigenesis and the development of CRPC (17–19). The positive associations among PTEN loss, AKT and MAPK signatures, and the NCoA2 signature prompted us to investigate whether NCoA2 exerts its functions partially through modulating PI3K/AKT and MAPK signaling in PCa. To this end, we performed Western blot and IHC assays to validate the above observations. Indeed, there was a significant increase of phospho-AKT and phospho-ERK levels in the prostate tumors of PTEN$^{PC+/-}$ NCoA2$^{PCOE/+}$ mice in compari-

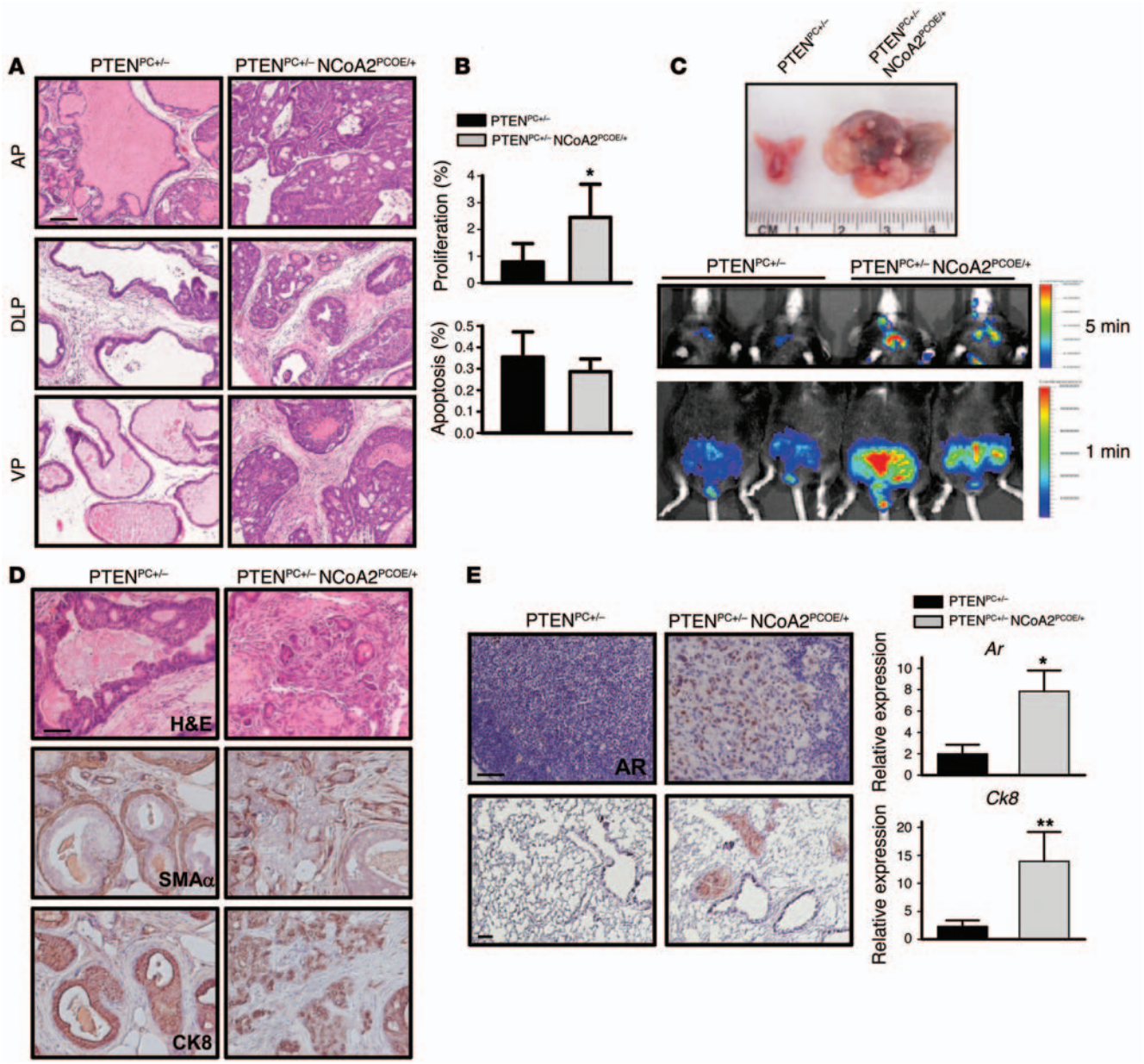

Figure 2. NCoA2 collaborates with PTEN loss to promote PCa progression and metastasis. (**A**) H&E-stained sections of representative AP, DLP, and VP at 6–7 months of age in PTEN$^{PC+/-}$ and PTEN$^{PC+/-}$ NCoA2$^{PCOE/+}$ mice. (**B**) The percentage of proliferating and apoptotic cells in PTEN$^{PC+/-}$ and PTEN$^{PC+/-}$ NCoA2$^{PCOE/+}$ mice at 6 months of age were determined using Ki67 and cleaved caspase 3 assays, respectively. (**C**) Top: Macroscopic dissection image of prostate isolate from PTEN$^{PC+/-}$ and PTEN$^{PC+/-}$ NCoA2$^{PCOE/+}$ mice. Representative images of luciferase-reporter activity of PTEN$^{PC+/-}$ and PTEN$^{PC+/-}$ NCoA2$^{PCOE/+}$ mice at 12 months of age are displayed. Middle: Luciferase activity of PCa cells that have metastasized to distant sites in the chest area (exposed for 5 minutes). Bottom: Luciferase activity in the prostate and surrounding area (exposed for 1 minute). (**D**) H&E-stained sections of DLP at 12 months of age and IHC analyses of α-SMA and CK8 in prostate tumors. (**E**) Left: AR expression in lumbar lymph nodes (top) and lungs (bottom) at 12 months of age. For quantitative results of metastatic incidence, see Table 1. Right: Relative mRNA levels of *Ar* and *Ck8* levels in lymph node from PTEN$^{PC+/-}$ and PTEN$^{PC+/-}$ NCoA2$^{PCOE/+}$ mice (n = 6). Scale bars: 50 μm (**A**, **D**, and **E**). *P < 0.05; **P < 0.01.

son with PTEN$^{PC+/-}$ mice (Figure 4B). The downstream effectors of PI3K/AKT signaling, phospho-S6 and phospho-GSK3β were simultaneously elevated in the prostate tumors isolated from PTEN$^{PC+/-}$ NCoA2$^{PCOE/+}$ mice. IHC analysis further supported the notion that NCoA2 serves as an upstream regulator to activate PI3K/AKT and MAPK signaling, as evidenced by the increase in phospho-AKT and phospho-ERK staining in NCoA2 overexpression mice (Figure 4C). To further investigate whether these genetic pathways identified could be observed in patients, we extended our examination by querying gene expression profiling datasets. As indicated in Figure 4D, both NCoA2 expression level and NCoA2 signature, as defined by gene expression profiles obtained from PTEN$^{PC+/-}$ NCoA2$^{PCOE/+}$ mice, were significantly elevated in patients with metastatic PCa in comparison with primary tumors, corroborating the notion that NCoA2 is critical for PCa metastasis. In addition, the pivotal roles of NCoA2 in

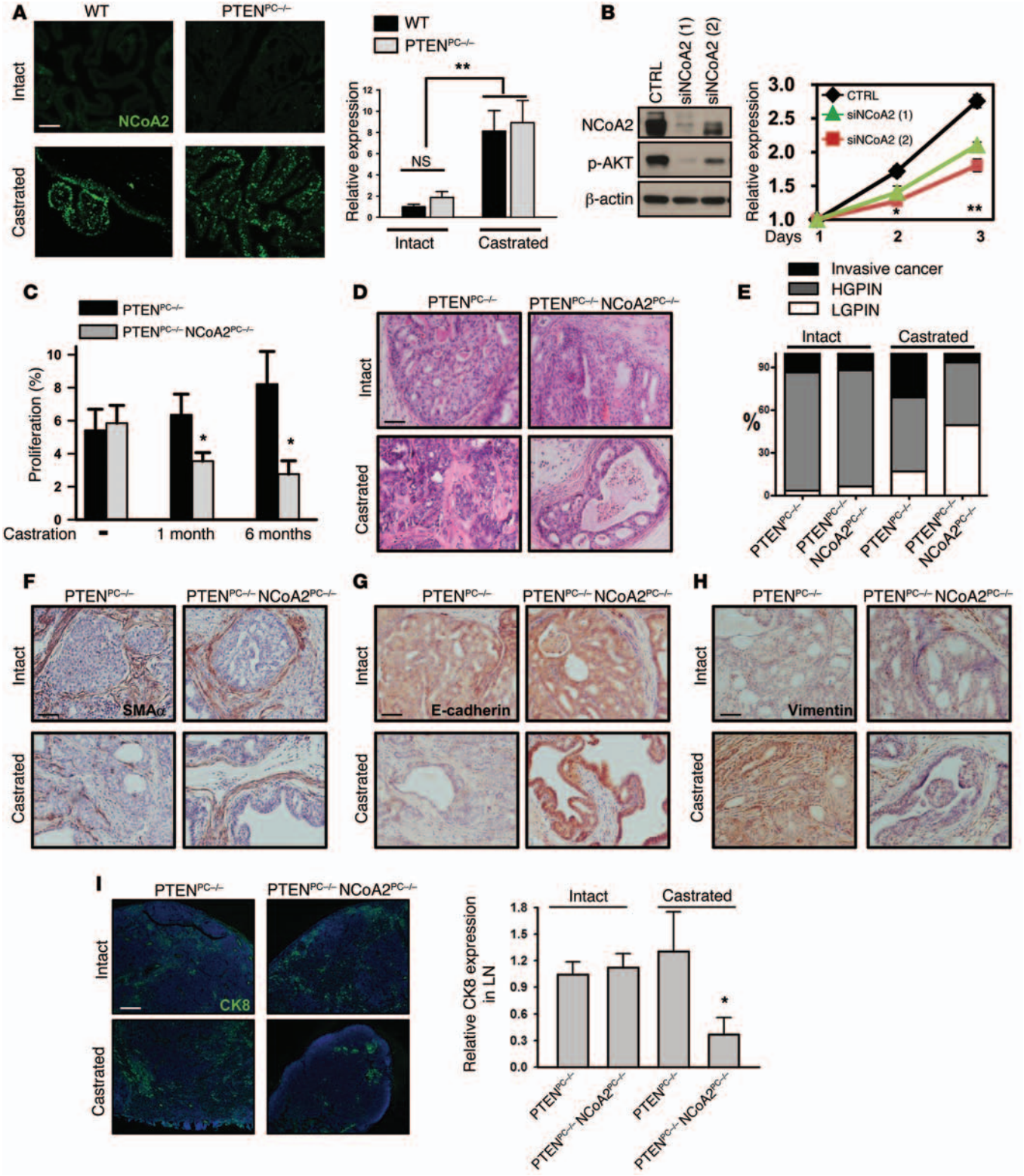

Figure 3. Upregulation of NCoA2 during androgen deprivation is critical in metastatic CPRC. (**A**) Immunostaining (left) and qRT-PCR (right) analysis of NCoA2 expression in wild-type and PTEN-null prostate with or without castration. $n = 10$. (**B**) MTT analysis of cell growth in CTRL and NCoA2-depleted LNCaP-Abl cells cultured in charcoal-stripped media. $n = 3$. (**C**) Quantitative results of Ki67-positive staining in prostate tumors from PTEN$^{PC-/-}$ and PTEN$^{PC-/-}$ NCoA2$^{PC-/-}$ mice after 1 or 6 months of castration. $n = 6$. (**D**–**H**) H&E staining (**D**); IHC analyses of α-SMA (**F**), E-cadherin (**G**), and vimentin (**H**) expression; and quantitative results (**E**) of prostate tumor progression in prostate tumors from PTEN$^{PC-/-}$ and PTEN$^{PC-/-}$ NCoA2$^{PC-/-}$ mice with or without castration (mice were castrated at 4 months of age, and the samples were isolated after 6 months of castration). $P < 0.001$ (invasive tumor and LGPIN), $P = 0.3218$ (HGPIN), castrated PTEN$^{PC-/-}$ vs. castrated PTEN$^{PC-/-}$ NCoA2$^{PC-/-}$, Fisher's exact test. (**I**) Lymph node metastasis of prostate tumors in PTEN$^{PC-/-}$ and PTEN$^{PC-/-}$ NCoA2$^{PC-/-}$ mice with or without castration are shown as above. qRT-PCR analysis of *Ck8* expression in lymph node was used to quantify metastasis. $n = 8$. Scale bars: 100 μm (**A** and **I**), 50 μm (**D**, **F**–**H**). $^*P < 0.05$; $^{**}P < 0.01$.

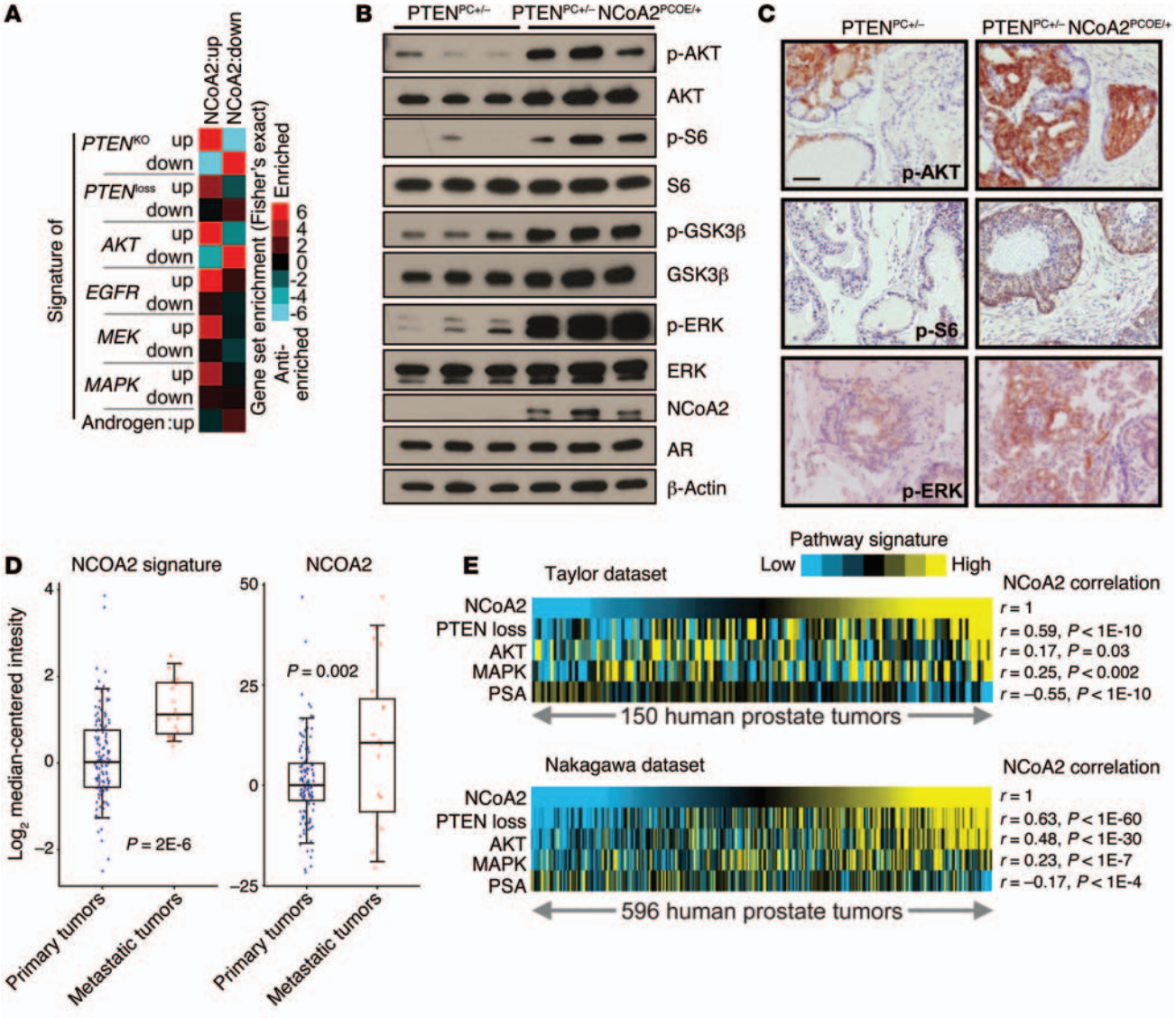

Figure 4. NCoA2 activates PI3K/AKT and MAPK signaling in PCa. (**A**) RNA profiling datasets, in which a particular pathway (AKT/PTEN, EGFR, MEK, MAPK, and AR) was activated in an experimental model, were collected from various published studies (described in Supplemental Table 1). Graphic representation of the significance of gene overlap is shown (Fisher's exact *z* score), for NCoA2-regulated genes, as defined by microarray from $PTEN^{PC+/-}$ $NCoA2^{PCOE/+}$ versus $PTEN^{PC+/-}$ mice, with the various external pathway signatures. (**B**) Western blot analysis of phospho-AKT, AKT, downstream targets (phospho-S6 and phospho-GSK3β), AR, phospho-ERK, and total ERK in anterior prostate from 24-week-old mice as indicated. (**C**) IHC analysis of phospho-AKT, phospho-S6, and phospho-ERK as indicated. Scale bars: 50 μm. (**D**) NCoA2 expression and NCoA2 signature in primary versus metastatic PCa specimens from patients (GSE21032; ref. 9), in which each tumor expression profile was scored for manifestation of the NCoA2 signature. Box plots represent 5%, 25%, 75%, median, and 95%. *P* values were examined using *t* test. (**E**) Pearson's correlations between NCoA2 signature and PTEN loss, AKT activation, MAPK, or androgen signature as reflected by PSA levels within primary prostate tumors (Taylor dataset, GSE21032, *n* = 150, ref. 9; Nakagawa dataset, GSE10645, *n* = 596, ref. 30).

mediating PI3K/AKT and MAPK signaling were also manifested by patient specimen analysis (Figure 4E). Consistent with the functional results obtained from GEMs, we observed a significant and positive correlation between NCoA2 and PTEN loss and activation of PI3K/AKT and MAPK signaling (using datasets GSE21032 and GSE10645; Figure 4E and refs. 9, 30). Collectively, these results further support the role of NCoA2 as an upstream regulator that activates PI3K/AKT and MAPK signaling in PCa.

Although NCoA2 has been shown to act as an AR coactivator to modulate its transcription activity (26), we did not observe a significant increase in androgen gene signature in NCoA2-overexpressing prostates (Supplemental Table 2). Consistent with this observation, results from qRT-PCR of classical AR downstream targets indicated that NCoA2 generally did not coactivate AR transactivation in a PTEN-mutated prostate. As shown in Supplemental Figure 7, up- or downregulation of NCoA2 did not alter the expression levels of classical downstream targets of androgen signaling. Instead, in PCa patients, AR signaling as reflected by the expression level of prostate-specific antigen (PSA) was negatively associated with the NCoA2 signature, consistent with the fact that AR serves as an upstream regulator to inhibit NCoA2 expression (Figure 4E and Supplemental Table 2). Taken together, these

results suggest that NCoA2 might regulate PI3K/AKT and MAPK signaling instead of coactivating androgen signaling to promote PCa progression.

NCoA2 directly regulates key components of PI3K/AKT and MAPK pathways to promote CRPC. To further dissect the molecular mechanism of NCoA2 action in CRPC, we immunoprecipitated chromatin from the dorsolateral prostate of 7-month-old $PTEN^{PC+/-}$ $NCoA2^{PCOE/+}$ mice and analyzed the precipitated DNA with deep sequencing. We identified 13,366 genes that harbor NCoA2 binding sites within 50 kb of their annotated gene margins (Supplemental Figure 8, A and B). This number was reduced to 7,620 if only binding sites within the extended promoter region (EPR; transcription start site [TSS] –7.5 kb to TSS +2.5 kb) were considered. Because analysis using the Cis-regulatory Element Annotation System (http://liulab.dfci.harvard.edu/CEAS/) identified approximately 20-fold enrichment of NCoA2 binding in promoter-proximal regions, we only used genes with ChIP binding in the EPR that showed changes in gene expression, to further identify 1,023 bona fide NCoA2 gene targets in this mouse model. Consistent with our transcriptome results, functional annotation analysis of the NCoA2 cistrome revealed enrichment of signaling pathways important for cancer, including "regulation of protein kinase activity" and "positive regulation of MAPK activity" (Supplemental Figure 8C). On a molecular basis, this analysis further supports the notion that NCoA2 plays pivotal roles in PCa progression and metastasis.

As the expression profile analysis indicated that NCoA2 profoundly stimulates PI3K/AKT and MAPK signaling, and these two signaling pathways are known to exert critical roles in PCa disease progression, we examined whether NCoA2 could be directly recruited to the key regulatory elements within these 2 pathways. ChIP-Seq analysis and further validation assays revealed that several NCoA2 genomic targets are commonly associated with the PI3K/AKT signaling pathways, such as *Phlpp1*, an AKT phosphatase, and *Fkbp5*, a heat shock protein that can stabilize *Phlpp1* and *Pten* genes (Figure 5A). These analyses suggest that NCoA2 may directly regulate the expression of *Phlpp1* and *Fkbp5* genes to control PI3K/AKT signaling. The immunophilin FKBP5 is a chaperone for the AKT phosphatase PHLPP; its expression in PCa is androgen dependent, and its downregulation results in decreased PHLPP protein stability and increased AKT phosphorylation (14, 17, 18). Here we found that NCoA2 was directly recruited to multiple sites within the *Fkbp5* and *Phlpp1* gene locus (Figure 5A). Further qRT-PCR and IHC assays validated that the expression of FKBP5 and PHLPP1 transcripts and protein was indeed reduced in $PTEN^{PC+/-}$ $NCoA2^{PCOE/+}$ mice (Figure 5C and Supplemental Figure 9C). Similarly, depletion of NCoA2 in PCa cells resulted in the upregulation of FKBP5 and PHLPP1 (Supplemental Figure 9, A and E). Furthermore, we conducted luciferase reporter assays and showed that NCoA2 indeed repressed *Fkbp5* promoter–driven reporter expression (Supplemental Figure 9B). Given that *FKBP5* is an androgen-responsive gene (31), we sought to determine whether the recruitment of NCoA2 to the *Fkbp5* gene locus was dependent upon AR. As shown in Supplemental Figure 11A, both AR and NCoA2 were recruited to region 2 (enhancer) and region 4 (within intron 5), whereas only NCoA2 bound to region 3, near the TSS (Supplemental Figure 10A). More importantly, we showed that NCoA2 recruitment to the *Fkbp5* locus was independent of AR status (Supplemental Figure 10, B and C). Though androgen depletion abolished AR binding to the *Fkbp5* locus (Supplemental Figure 10B), it did not alter recruitment of NCoA2, suggesting that NCoA2 regulates FKBP5 expression in an AR-independent manner (Supplemental Figure 10C). Interestingly, we also identified that NCoA2 was directly recruited to the proximal promoter region of the *Pten* gene locus (Figure 5A) and repressed the expression of a *Pten* promoter–driven reporter that contains the NCoA2 binding region (Supplemental Figure 9D). Functional assays indicated that depletion of NCoA2 stimulated PTEN expression in PTEN wild-type VCaP cells (Supplemental Figure 9E), whereas overexpression of NCoA2 downregulated PTEN levels in prostate tumors (Supplemental Figure 9F). Taken together, these results indicate that NCoA2 negatively and directly regulates the *Fkbp5*, *Phlpp1*, and *Pten* genes at the transcriptional level and thereby modulates the PI3K/AKT signaling pathway.

ChIP-Seq and subsequent analysis via qRT-PCR and Western blot assays showed that NCoA2 also binds to and controls the expression of genes that participate in MAPK signaling, such as *Map3k1* (also known as MAPK/ERK kinase kinase 1, or *Mekk1*) and *Rac-GEF* (PIP3-dependent Rac-GTPase exchange factor, or *Prex1*), a Ras family guanine nucleotide exchange factor activating Ras and the RAF-MEK-ERK pathway (Figure 5, B and C, and Supplemental Figure 11). Taken together, our results show that NCoA2 activates PI3K/AKT and MAPK pathways through direct regulation of a broad spectrum of key genes in the AKT and MAPK signaling pathways.

Previous studies suggested that AR inhibition destabilizes PHLPP1 through inhibition of FKBP5 expression and thereby provokes unchecked AKT activation, leading to CRPC in PTEN-null tumors (17, 18). We thus examined whether activation of PI3K/AKT and MAPK signaling in our NCoA2 mouse model is also an underlying cause for CRPC. As shown in Figure 5, D–F, concomitant with the reduction of FKBP5 and PHLPP1 expression, the prostate tumors isolated from castrated $PTEN^{PC-/-}$ mice displayed a significant increase in phospho-AKT levels compared with intact $PTEN^{PC-/-}$ mice. In sharp contrast, ablation of NCoA2 in castrated PTEN-null mice enhanced both FKBP5 and PHLPP1 expression, leading to the reduction of AKT activation. Likewise, ablation of NCoA2 in castrated PTEN-null tumors decreased the activity of MAPK signaling as reflected by the reduction of phospho-ERK levels (Supplemental Figure 12). Taken together, our results indicated that NCoA2 potentiates the PTEN-null tumors to develop CRPC at least partially through direct regulation of the PTEN/FKBP5/PHLPP1/AKT signaling cascade and MAPK signaling.

Finally, to investigate the biological significance of NCoA2 in patients, we extended our examination by querying gene expression profiling dataset GSE10645 (30) (comprising 596 primary tumors with PCa-specific death and PSA recurrence information), and scoring each of the human tumor profiles for NCoA2 activity, using the gene signature from our mouse model. We observed distinct differences over time in PCa-specific death and PSA recurrence among patients with higher versus lower inferred NCoA2 activity (Figure 6A), thus supporting a pivotal role of NCoA2 in PCa.

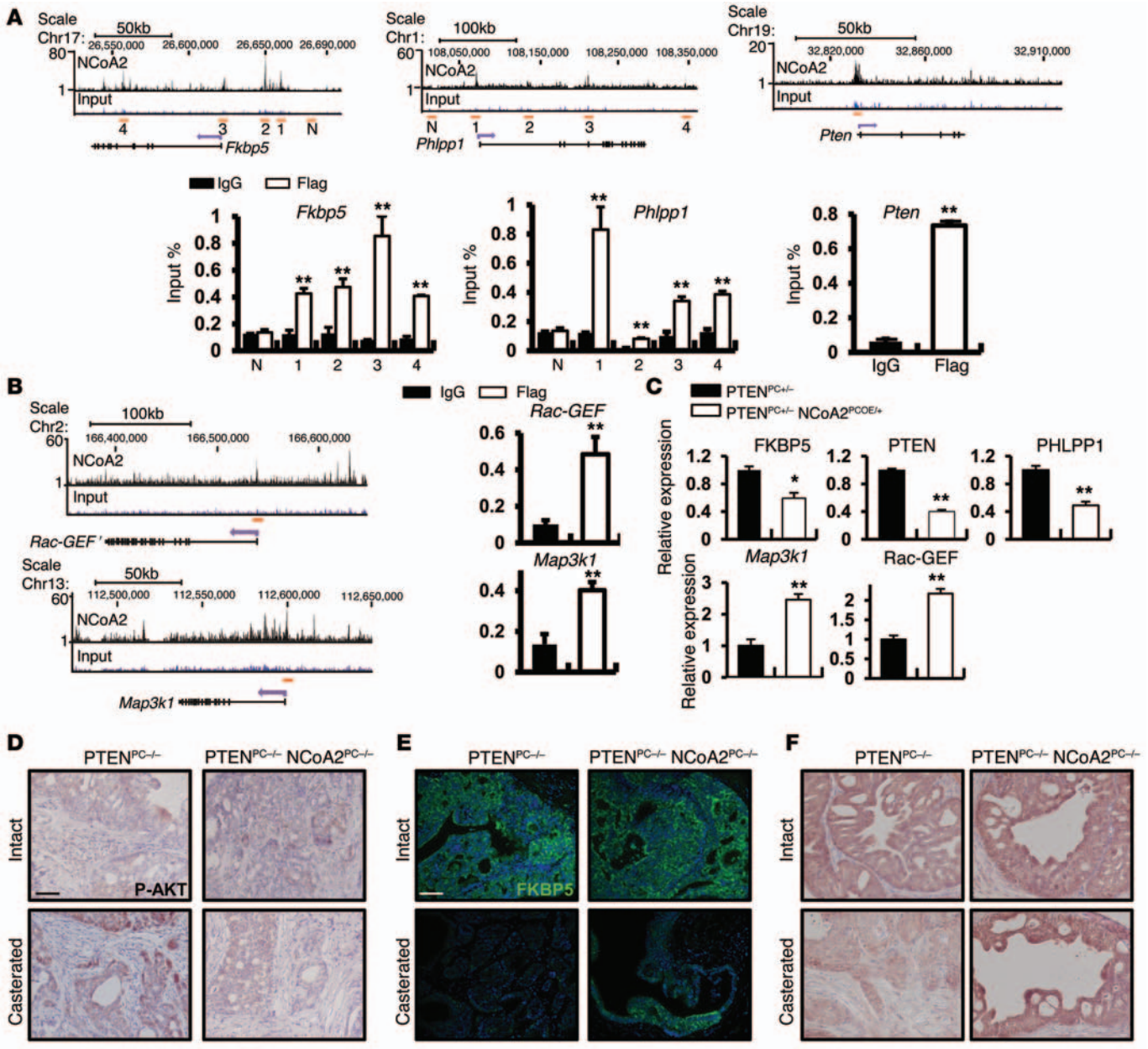

Figure 5. NCoA2 directly regulates key components of PI3K/AKT and MAPK pathways to promote CRPC. (**A**) ChIP-seq results of NCoA2 binding in the *Fkbp5*, *Phlpp1*, and *Pten* locus. Numbers indicate NCoA2 binding sites (top). N indicates a region without NCoA2 binding sites that served as a negative control. ChIP-PCR assays for NCoA2 binding to *Fkbp5*, *Phlpp1*, and *Pten* genes on pooled 7-month-old PTEN$^{PC+/-}$ NCoA2$^{PCOE/+}$ prostate samples using anti-Flag antibody (NCoA2 with Flag tag) or IgG (bottom). Bar graphs show an enrichment of DNA fragments pulled down by anti-Flag antibodies. (**B**) Left: ChIP-seq result of NCoA2 binding in the *Map3k1* and *Rac-GEF* locus. Right: ChIP-PCR assays for NCoA2 binding to *Map3k1* and *Rac-GEF* genes are as denoted. (**C**) Relative mRNA levels of denoted genes from PTEN$^{PC+/-}$ and PTEN$^{PC+/-}$ NCoA2$^{PCOE/+}$ prostates (n = 6). (**D**–**F**) IHC analysis of phospho-AKT (**D**), FKBP5 (**E**) and PHLPP1 (**F**) expression in prostate tumors isolated from PTEN$^{PC-/-}$ and PTEN$^{PC-/-}$ NCoA2$^{PC-/-}$ mice with or without castration (6 months after castration). Student's t test was used for all the statistical analysis. Scale bars: 50 μm (**D**–**F**). $^*P < 0.05$; $^{**}P < 0.01$.

Discussion

Present studies highlight a critical role of NCoA2 in driving full malignant progression of PTEN-deficient PCa and CRPC. Given the fact that NCoA2 is frequently amplified or overexpressed in metastatic PCa patients, our studies uncovered a novel paradigm for combination therapy that is highly clinically relevant. Patients characterized by NCoA2 overexpression are likely to quickly develop CRPC; thus, combination treatment strategy employing ADT together with inhibitors of PI3K/AKT and MAPK signaling may likely have a beneficial effect.

Previous studies have shown that the inhibition of FKBP5/PHLPP-mediated negative feedback to AKT activation as a result of ADT enhances the strength of the PI3K/AKT pathway and contributes to androgen-independent growth (17, 18). However, the underlying mechanism for how ADT elicits the activation of PI3K/AKT signaling remains largely elusive. Here we identified

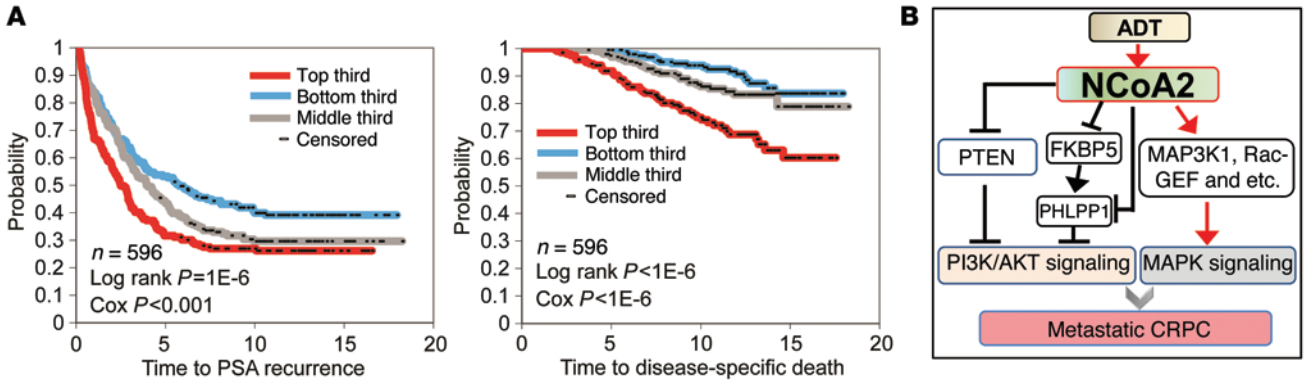

Figure 6. Role of NCoA2 in PCa. (**A**) Kaplan-Meier plot indicates the association of NCoA2 signature with PSA recurrence and disease-specific death in patients with PCa (using dataset GSE10645; ref. 30), with the top third, middle third, and bottom third of patients representing inferred NCoA2 activities from high to low (*P* values by log-rank test and univariate Cox). (**B**) Model of NCoA2 in prostate tumorigenesis. ADT induces NCoA2 expression, which in turn activates PI3K/AKT signaling (via negative regulation of FKBP5, PHLPP1, and PTEN) and MAPK signaling (via positive regulation of MAP3K1, Rac-GEF, and others) that together promote PCa metastasis and CRPC.

that NCoA2 serves as a pivotal integrator that regulates PI3K/AKT and AR signaling crosstalk to promote PCa metastasis and CRPC development. NCoA2 expression is significantly induced upon androgen deprivation, which consequently represses the expression of FKBP5 and destabilizes PHLPP1 to augment AKT signaling (Figure 6B). In addition, NCoA2 directly inhibits the expression of PTEN and PHLPP1 to further enhance AKT signaling. The critical role of PTEN in PCa is well established, and the clinical relevance and pathological roles of FKBP5 and PHLPP1 in PCa have been uncovered in recent years. PHLPP protein has emerged as a key player in PCa and exhibits tumor suppressor activity in this disease (14, 18). Similarly, FKBP5 functions as a scaffolding protein that enhances the PHLPP-AKT interaction and facilitates PHLPP-mediated dephosphorylation of AKT-Ser473 (31, 32). Therefore, FKBP5 also functions as a tumor suppressor, similar to the role of PTEN in PCa. Consistent with these findings, the present studies highlight the critical and tightly orchestrated roles of the tumor suppressors PTEN, PHLPP1, and FKBP5 in the development of CRPC, and uncover NCoA2 as an integrator that regulates the signaling circuits involved in this disease (Figure 6B).

Patients who have failed ADT often display augmented phospho-MAPK levels (33), indicating a feedback activation of MAPK signaling during the development of CRPC. Accordingly, GEMs demonstrate that the RAS/MAPK pathway collaborates with PTEN deficiency in promoting metastasis and CRPC development (19). Here we also identified that NCoA2 stimulates MAPK signaling through upregulation of *Rac-GEF* and *Map3k1* (Figure 6B). Rac is a subfamily of the Rho family of small GTPases, which mediates MAPK pathway activity (34). *Rac-GEF*, an activator of Rac proteins by catalyzing the exchange of GDP for GTP, has been shown to correlate with metastatic phenotype in various types of cancers including PCa (35–37). The increased expression of *Rac-GEF* and *Map3k1*, a MAPK kinase kinase, by NCoA2 upon androgen deprivation contributes to the activation of MAPK signaling and consequently enhances PTEN-deficient tumor malignancy.

The negative association between AR signaling and NCoA2 signature in patients is consistent with the notion that AR serves as an upstream regulator to inhibit NCoA2 transcription. Notably, our transcriptome analysis and further validation assays suggest that NCoA2 generally did not coactivate AR transcription at least in PTEN-mutated prostates. Furthermore, changes in NCoA2 expression in mice and cells also did not affect AR expression. Further studies will be needed to systematically analyze whether androgen signaling is involved in NCoA2-mediated circuits to induce CRPC.

Though NCoA2 presumably serves as a coactivator for gene transcription, evidence has revealed that NCoA2 also acts as a co-repressor to inhibit gene expression in a context-dependent manner (38, 39). This context could be established by epigenetic modulation of chromatin structure, through tethering of NCoA2 to different transcription factors, through dynamic posttranslational modification of NCoA2 under various stimulants, or via other mechanisms. For instance, recent studies indicate that NCoA2 is equally recruited to glucocorticoid receptor (GR) binding sites to activate or repress GR-downstream genes under inflammation insults (38). The present studies also found that NCoA2 can activate (*Map3k1* and *Rac-GEF*) or repress (*Phlpp1*, *Fkbp5*, and *Pten*) gene transcription in a context-dependent manner. The mechanism that underlies the switching of NCoA2 from a coactivator to a co-repressor remains to be elucidated. In addition, since NCoA2 does not directly bind to DNA, it is currently unclear which transcription factor(s) cooperates with NCoA2 to promote prostate tumorigenesis. Interestingly, motif analysis of NCoA2 binding sites in the ChIP-Seq data revealed a significant enrichment of ETS, GATA, and JUN transcription factors, which have been shown to be crucial regulators in prostate tumorigenesis. Whether NCoA2 interacts with these transcription factors to promote PCa progression remains to be determined.

Finally, we note the potential caveat of using an overexpression approach in this study. To address this issue, we compared NCoA2 levels in the overexpression mice with a panel of human PCa cell lines and normal prostate epithelial cells (RWPE-1). Consistent with patient data, NCoA2 expression was upregulated in PCa cells except for LNCaP cells, which have intact androgen signals to suppress NCoA2 expression (Figure 1C). More importantly, the expression level of NCoA2 in the overexpression mice

was comparable to its abundance in prostate cancer cells including LNCaP-Abl, DU145, and 22RV-1 cells (Figure 1C). In addition, given the fact that NCoA2 expression in the intact prostate is suppressed by androgen signaling, we also examined its expression in castrated mice. As shown in Figure 1D, the expression levels between wild-type castrated mice and NCoA2 overexpression mice were found to be within the same range. Furthermore, NCoA2 levels in the overexpression mice were found to be comparable with those observed in other tissues that have higher endogenous NCoA2 levels, such as the testes and uterus in wild-type mice (Figure 1C). Taken together, these results indicate that the NCoA2 overexpression mouse model used in this study can largely reflect the pathological conditions in PCa. Our studies thus provide a new conceptual framework with which to investigate how NCoA2 mediates PI3K/AKT/MAPK and AR pathway crosstalk as a mechanism of PCa metastasis and CRPC development, with important implications for PCa therapy.

Methods

Animal experiments. The Flag-tagged NCoA2$^{OE/+}$ mice were generated by our group using a similar approach as previously described (40). *Ncoa2*$^{fl/fl}$ mice (21) were originally from P. Chambon (Institute for Genetics and Cellular and Molecular Biology, Strasbourg, France). *Pten*$^{fl/fl}$ mice (3) were originally from H. Wu (UCLA, Los Angeles, California, USA). The *Arr2pb-Cre* (probasin-*Cre*; PB-Cre) transgenic mice (27) were from F. Wang (Institute of Bioscience and Technology, Texas A&M Health Science Center, Houston, Texas, USA). The Luciferase^{OE} (Rosa26-pCAGGs-LSL-Luciferase) reporter mice were from mouse repositories at NCI at Frederick (Frederick, Maryland, USA). All the mice were backcrossed with C57BL/6 mice for at least 5 generations and maintained according to the NIH *Guide for the Care and Use of Laboratory Animals*. NCoA2$^{OE/+}$ or *Ncoa2*$^{fl/fl}$ mice were first crossed with *Pten*$^{fl/fl}$ mice. The resulting compound mice were then crossed with probasin-*Cre* mice for conditional knockout or overexpression of NCoA2 in the prostate epithelium. Castration surgery was performed as previous described (17). In brief, 4-month-old male mice were anesthetized by i.p. injection of Avertin (2.5% in saline, 15 μl/g body weight). Mice were castrated via a scrotal incision. Luciferase bioluminescence assay was performed using Xenogen 200 In Vivo Imaging System (IVIS) according to the manufacturer's instructions. In brief, mice were anesthetized by isoflurane inhalation, and 100 mg/kg D-luciferin/DPBS was injected i.p. 5 minutes before imaging.

Expression plasmids, siRNA, and cell cultures. The full-length human *NCOA2* cDNA was cloned into pMSCV-puro/neo (Clontech), pcDNA5 (Flag tag) (Invitrogen), and pcDNA3.1 (Myc tag) to generate NCoA2 expression plasmids. SMART pool or single siRNA duplexes targeting NCoA2, AR, and control non-target siRNA were purchased from Dharmacon. LNCaP, PC3, DU145, and LNCaP-Abl cells were obtained from the Tissue & Cell Culture Core Facility at Baylor College of Medicine. LNCaP, PC3, and DU145 cells were cultured in RPMI supplemented with 10% FBS; LNCaP-Abl cells were culture in 10% charcoal-stripped serum (CSS). Cells were transfected with siRNA duplexes (40–80 nM) using Lipofectamine 2000 (Invitrogen) or Dharmacon Transfection (Dharmacon) reagents according to the manufacturer's instructions. Flag-tagged NCoA2 overexpression lentivirus was generated and transfected as previously described (13). Briefly, cells were transduced with lentivirus and cultured with puromycin at 1 μg/ml, and the selection was stopped as soon as the non-infected control cells died off. The cell proliferation assay was performed using a CellTiter 96 Non-Radioactive Cell Proliferation Assay (MTS) kit (Promega) following the manufacturer's instructions. Results were calculated based on 3 independent experiments, and statistical significance was determined by 2-sided Student's *t* test. Luciferase reporter assays were carried out as previously described (13). Briefly, 48 hours after transfection, cells were harvested for measurement of luciferase and β-galactosidase activities. All assays were done in duplicate, and all values were normalized for transfection efficiency against β-galactosidase activities. Luciferase activity was determined using the Promega luciferase assay kit. Results were quantified based on 3 independent experiments, and statistical significance was determined by 2-sided Student's *t* test. $P < 0.05$ was considered statistically significant.

RNA isolation and RT-PCR. Total RNA was extracted using TRIzol reagent according to the manufacturer's instructions. First-strand cDNA was synthesized using 2 μg total RNA and Maxima cDNA synthesis kit (Thermo Scientific). FastStart Universal SYBR Green Master (Rox) reagent (Roche) was used for qPCR, and reaction was performed using the StepOnePlus Real-time PCR System (Applied Biosytems). The level of gene expression was obtained using the ΔΔCt method, in which all samples are first normalized to the level of β-actin in each sample. The Student's *t* test was used for statistical analysis of qRT-PCR results, and *P* values less than 0.05 were considered significant. Primer sequences are indicated in Supplemental Table 3.

Histology and IHC. The ventral, dorsolateral, and anterior prostate lobes were dissected, fixed in 4% formaldehyde in PBS for 24 hours, processed, and embedded in paraffin. Sections (7 μm) were processed using H&E staining. Prostate hyperplasia was characterized by the proliferation of lumina with no cytological atypia containing small foci with 2 or 3 layers of cells. Those PIN lesions were graded using the nomenclature and criteria developed by Park et al. (41). Basically, HGPIN is characterized by an intraglandular proliferation of crowding cells with atypia, and cribriform formation or the development of multilayered solid glandular structures. Invasive adenocarcinoma is characterized by the proliferation of atypical cells that break the basal membrane and invade through the prostatic stroma. The quantitative results of tumor progression are from random 2 slides of each mouse in a total 6–8 pairs of PTEN$^{PC+/-}$ and PTEN$^{PC+/-}$ NCoA2$^{PCOE/+}$ mice or PTEN$^{PC-/-}$ and PTEN$^{PC-/-}$ NCoA2$^{PC-/-}$ mice (with or without castration). Once prostate acini developed adenocarcinoma, we considered the mouse positive for adenocarcinoma, hyperplasia, and HGPIN. For IHC, the slides were processed using citrate buffer–based (pH 6.0) antigen retrieval and the avidin-biotin peroxidase IHC method. Sections were counterstained with DAPI (Sigma-Aldrich). Quantification of tumor malignancy was done as follows: for Ki67-staining, positive cells were counted after imaging with a Zeiss Axioplan microscope. Three random slides of each animal were counted. Proliferative rate was determined by counting the number of proliferating (Ki67-positive) cells in a total of 100 cells, and the statistical significance was determined using a 2-tailed Student's *t* test. For lymph node metastasis, we performed CK8 or AR immunostaining in lymph nodes or lungs and recorded the percentage of mice with positive staining, which was considered to indicate lymph node or lung metastasis. For invasive adenocarcinoma identification, we

performed α-SMA immunostaining. If the gland or acini displayed a loss or breakdown of the continuous layer of basal membrane (α-SMA positive) and the appearance of AR- or CK8-positive epithelial cells invading into the stromal compartment, we consider microinvasive cancer to have developed. The statistical significance between groups was determined using a 2-tailed Fisher's exact test, and *P* values less than 0.05 were considered significant.

Western blotting and immunostaining. Total proteins were extracted from cells following standard protocol (42). Protein concentration was measured using a BCA Protein Assay Kit (Thermo Scientific). HRP-conjugated secondary antibodies were purchased from DAKO. Signals were visualized with Super Signal West Pico Chemiluminescent Substrate Kit (Pierce). Paraffin-embedded prostate tissue sections were processed for immunostaining as previously described. Immunostaining was performed using a Vector M.O.M. Peroxidase kit, followed by DAB substrate (Vector) for light microscopy and Alexa Fluor 488 tyramide TSA kit #22 (Invitrogen) for fluorescence microscopy according to the manufacturer's instructions. All primary antibodies used in this study were purchased from Cell Signaling, except for AR (Santa Cruz), CK8 (Covance), α-SMA (Sigma-Aldrich), NCoA2 (Bethyl Laboratories), FKBP5 (Abcam), PHLPP1 (Millipore), Rac-GEF (Millipore), E-cadherin (BD), Vimentin (BD), and β-actin (Sigma-Aldrich).

ChIP assay. Mouse prostate tissue was collected from 7-month-old *PTEN*$^{PC+/-}$ *NCoA2*$^{OE/+}$ mice. Tissue chromatin was prepared and followed by ChIP-Seq analysis (Active Motif Inc.) using the antibody against NCoA2 (A300-346A; Bethyl Laboratories). Thirty-one million reads were mapped to the mouse genome (Build37_1/mm9) using BWA software to yield 10,863,308 unique alignments. At a MACS cut-off of $P = 1 \times 10^{-7}$, 12,094 intervals were identified over input control. Fifteen negative peaks were noticed that produced a false discovery rate of 0.12%. The average NCoA2 ChIP-Seq-interval length was 1,159 bp; raw data were deposited in GEO (accession no. GSE54770). The tissue chromatin for ChIP-qPCR assay was the same as that in the ChIP-Seq analysis prepared by Active Motif Inc. ChIP was performed as described previously (43) following the protocol provided by Millipore and using anti-Flag M2 antibody (Sigma-Aldrich). SYBR Green–based qPCR was then performed, and the enrichment of peaks was represented as percentage of input using standard curve method. Standard curves were generated by serial dilution of input. All the results were obtained from 3 repeats, and statistical significance was determined with a Student's *t* test. *P* values less than 0.05 were considered significant. Primer sequences were indicated in Supplemental Table 3.

Microarray analysis. For microarray analysis, total RNA was isolated from the dorsolateral prostate of 7-month-old control PTEN$^{PC+/-}$ and PTEN$^{PC+/-}$ NCoA2$^{PCOE/+}$ mice. Total RNA was extracted using TRIzol reagent (Invitrogen) followed by RNeasy Mini kit (Qiagen) cleanup according to the manufacturer's instructions. The Microarray Core at Baylor College of Medicine performed the microarray hybridization with Affymetrix GeneChip Mouse 430 2.0 arrays. Gene information for all probes was annotated based on "Mouse430_2.annot.csv," downloaded from the Affymetrix website. Data were analyzed with Microarray Suite version 5.0 (MAS 5.0) using Affymetrix default analysis settings and global scaling as the normalization method. The list of significance was operated by setting a false discovery rate threshold at level of 0.05. All differentially expressed gene lists generated as described above were further analyzed with Ingenuity Pathways Analysis (http://www.ingenuity.com/index.html) to identify canonical pathways and molecular and cellular functions enriched in the related gene lists. All raw data from the present expression array study were deposited in GEO (accession no. GSE54678).

Pathway analysis in NCoA2-overexpressing prostate. RNA profiling datasets, in which a particular pathway (AKT/PTEN, EGFR, MEK, MAPK, and AR) was activated in an experimental model, were collected from various published studies (described in Supplemental Table 1); the significance of gene overlap, between NCoA2-regulated genes (as defined by microarray from PTEN$^{PC+/-}$ NCoA2$^{PCOE/+}$ versus PTEN$^{PC+/-}$ mice) and the various external pathway signatures, was computed using Fisher's exact tests (only genes represented on the 430_2 array platform were used in the calculation).

Analysis of NCoA2 signature in patients with PCa. Scoring of human tumor expression profiles, using an external gene signature, was carried out essentially as previously described (13, 44–49). For analysis in human tumor datasets, the NCoA2 signature was derived from our own gene expression profile dataset of *Pten* heterozygous mutation mouse prostate with or without NCoA2 overexpression. The NCoA2 gene signature (defined using fold change > 1.5 for each NCoA2 overexpression sample profile versus control sample profile) consisted of 1,131 unique human orthologous genes induced with NCoA2 overexpression and 985 genes repressed. In order to define the degree of NCoA2 gene signature manifestation within profiles from an external human tumor dataset (e.g., GSE10645), we used the previously described *t* score metric (45, 50). Briefly, the *t* score was defined for each external profile as the 2-sided *t* statistic comparing, within the profile, the average of the NCoA2-induced genes with the average of the NCoA2-repressed genes (genes within the human tumor dataset were first centered to standard deviations from the median of the primary tumor specimens). The GSE10645 mRNA profile dataset consisted of genes in a focused panel of 891 (using the combined "Human Cancer" and "Human Custom" panels, which did not include *NCOA2* mRNA itself), of which 168 were represented in our NCoA2 signature. For a given dataset, the *t* score contrasted the patterns of the NCoA2-induced genes against those of the NCoA2-repressed genes, in order to derive a single value denoting coordinate expression of the 2 gene sets. The Univariate Cox proportional hazard analysis and Kaplan-Meier survival analysis were used to determine the correlation of NCoA2 signature manifestation with patient outcome.

Statistics. Unless otherwise indicated, data in the figures are presented as mean ± SEM, and significant differences between experimental groups were determined using the 2-tailed Student's *t* test. The development of tumor metastasis and HGPIN in control and experimental groups and pathways analyzing in NCoA2-overexpressing prostate were calculated with the Fisher's exact test. A log-rank test was performed to compare patient survival and recurrence. All *P* values reported were 2-sided unless otherwise specified. A *P* value less than 0.05 was considered statistically significant.

Study approval. All animal experiments were approved by the Animal Center for Comparative Medicine at Baylor College of Medicine. All human cell lines used herein were standard cell lines available in ATCC.

Acknowledgments

We thank Wen Chen and Pei Li for technical support and Li-Yuan Yu-Lee for comments. We thank the Baylor Microarray Core supported by Durham Economic Resource Center (grant P30

DK079638) and Duncan Cancer Center for microarray analysis. We also thank Baylor Genetically Engineered Mouse Core for the service of mouse generation. This work was supported by grants from the NIH (DK59820 and HL114539), the Prostate Cancer Foundation, the Cancer Protection and Resource Institute of Texas (RP130315 to S.Y. Tsai and M.-J. Tsai), the NIDDK (DK45641 to M.-J. Tsai), the National Natural Science Foundation of China (31471281 and 81422030 to J. Qin), and the Science and Technology Commission of Shanghai Municipality (grant 14140901500 to J. Qin). The authors acknowledge the participation of the Adrienne Helis Malvin Medical Research Foundation through its direct engagement in the continuous active conduct of medical research in conjunction with Baylor College of Medicine and the Cancer Program.

Address correspondence to: Jun Qin, Institute of Health Sciences, Shanghai Institutes for Biological Sciences, Chinese Academy of Sciences & Shanghai Jiao Tong University School of Medicine, Shanghai, China. Phone: 86.21.54923326; E-mail: qinjun@sibs.ac.cn. Or to: Sophia Y. Tsai or Ming-Jer Tsai, Department of Molecular and Cellular Biology, Baylor College of Medicine, One Baylor Plaza, Houston, Texas 77030, USA. Phone: 713.798.6251; E-mail: stsai@bcm.edu (S.Y. Tsai). Phone: 713.798.6253; E-mail: mtsai@bcm.edu (M.-J. Tsai).

1. American Cancer Society. *Cancer Facts & Figures 2010*. Atlanta, Georgia, USA: American Cancer Society; 2010.
2. Shen MM, Abate-Shen C. Molecular genetics of prostate cancer: new prospects for old challenges. *Genes Dev*. 2010;24(18):1967–2000.
3. Wang S, et al. Prostate-specific deletion of the murine Pten tumor suppressor gene leads to metastatic prostate cancer. *Cancer Cell*. 2003;4(3):209–221.
4. Chen Z, et al. Crucial role of p53-dependent cellular senescence in suppression of Pten-deficient tumorigenesis. *Nature*. 2005;436(7051):725–730.
5. Tomlins SA, et al. Recurrent fusion of TMPRSS2 and ETS transcription factor genes in prostate cancer. *Science*. 2005;310(5748):644–648.
6. Lei Q, et al. NKX3.1 stabilizes p53, inhibits AKT activation, blocks prostate cancer initiation caused by PTEN loss. *Cancer Cell*. 2006;9(5):367–378.
7. Carver BS, et al. Aberrant ERG expression cooperates with loss of PTEN to promote cancer progression in the prostate. *Nat Genet*. 2009;41(5):619–624.
8. King JC, et al. Cooperativity of TMPRSS2-ERG with PI3-kinase pathway activation in prostate oncogenesis. *Nat Genet*. 2009;41(5):524–526.
9. Taylor BS, et al. Integrative genomic profiling of human prostate cancer. *Cancer Cell*. 2010;18(1):11–22.
10. Tomlins SA, et al. Integrative molecular concept modeling of prostate cancer progression. *Nat Genet*. 2007;39(1):41–51.
11. Trotman LC, et al. Pten dose dictates cancer progression in the prostate. *PLoS Biol*. 2003;1(3):E59.
12. Ding Z, et al. SMAD4-dependent barrier constrains prostate cancer growth metastatic progression. *Nature*. 2011;470(7333):269–273.
13. Qin J, et al. COUP-TFII inhibits TGF-beta-induced growth barrier to promote prostate tumorigenesis. *Nature*. 2013;493(7431):236–240.
14. Chen M, et al. Identification of PHLPP1 as a tumor suppressor reveals the role of feedback activation in PTEN-mutant prostate cancer progression. *Cancer Cell*. 2011;20(2):173–186.
15. Walsh PC, DeWeese TL, Eisenberger MA. Clinical practice. Localized prostate cancer. *N Engl J Med*. 2007;357(26):2696–2705.
16. Macfarlane RJ, Chi KN. Research in castration-resistant prostate cancer: what does the future hold? *Curr Oncol*. 2010;17(suppl 2):S80–S86.
17. Carver BS, et al. Reciprocal feedback regulation of PI3K and androgen receptor signaling in PTEN-deficient prostate cancer. *Cancer Cell*. 2011;19(5):575–586.
18. Mulholland DJ, et al. Cell autonomous role of PTEN in regulating castration-resistant prostate cancer growth. *Cancer Cell*. 2011;19(6):792–804.
19. Mulholland DJ, et al. Pten loss and RAS/MAPK activation cooperate to promote EMT and metastasis initiated from prostate cancer stem/progenitor cells. *Cancer Res*. 2012;72(7):1878–1889.
20. Matsumoto H, et al. Cotargeting androgen receptor and clusterin delays castrate-resistant prostate cancer progression by inhibiting adaptive stress response and AR stability. *Cancer Res*. 2013;73(16):5206–5217.
21. Gehin M, Mark M, Dennefeld C, Dierich A, Gronemeyer H, Chambon P. The function of TIF2/GRIP1 in mouse reproduction is distinct from those of SRC-1 p/CIP. *Mol Cell Biol*. 2002;22(16):5923–5937.
22. Chopra AR, et al. Absence of the SRC-2 coactivator results in a glycogenopathy resembling Von Gierke's disease. *Science*. 2008;322(5906):1395–1399.
23. Chopra AR, et al. Cellular energy depletion resets whole-body energy by promoting coactivator-mediated dietary fuel absorption. *Cell Metab*. 2011;13(1):35–43.
24. Reineke EL, et al. SRC-2 coactivator deficiency decreases functional reserve in response to pressure overload of mouse heart. *PLoS One*. 2013;7(12):e53395.
25. Stashi E, et al. SRC-2 is an essential coactivator for orchestrating metabolism circadian rhythm. *Cell Rep*. 2014;6(4):633–645.
26. Agoulnik IU, et al. Androgens modulate expression of transcription intermediary factor 2, an androgen receptor coactivator whose expression level correlates with early biochemical recurrence in prostate cancer. *Cancer Res*. 2006;66(21):10594–10602.
27. Jin C, McKeehan K, Wang F. Transgenic mouse with high Cre recombinase activity in all prostate lobes, seminal vesicle, and ductus deferens. *Prostate*. 2003;57(2):160–164.
28. Tuveson DA, et al. Endogenous oncogenic K-ras(G12D) stimulates proliferation widespread neoplastic developmental defects. *Cancer Cell*. 2004;5(4):375–387.
29. Creighton CJ. Multiple oncogenic pathway signatures show coordinate expression patterns in human prostate tumors. *PLoS One*. 2008;3(3):e1816.
30. Nakagawa T, et al. A tissue biomarker panel predicting systemic progression after PSA recurrence post-definitive prostate cancer therapy. *PLoS One*. 2008;3(5):e2318.
31. Brognard J, Newton AC. PHLiPPing the switch on Akt and protein kinase C signaling. *Trends Endocrinol Metab*. 2008;19(6):223–230.
32. Pei H, et al. FKBP51 affects cancer cell response to chemotherapy by negatively regulating Akt. *Cancer Cell*. 2009;16(3):259–266.
33. Suzuki A, Nakano T, Mak TW, Sasaki T. Portrait of PTEN: messages from mutant mice. *Cancer Sci*. 2008;99(2):209–213.
34. Jaffe AB, Hall A. Rho GTPases: biochemistry and biology. *Annu Rev Cell Dev Biol*. 2005;21:247–269.
35. Ebi H, et al. PI3K regulates MEK/ERK signaling in breast cancer via the Rac-GEF, P-Rex1. *Proc Natl Acad Sci U S A*. 2013;110(52):21124–21129.
36. Pandiella A, Montero JC. Molecular pathways: P-Rex in cancer. *Clin Cancer Res*. 2013;19(17):4564–4569.
37. Fine B, et al. Activation of the PI3K pathway in cancer through inhibition of PTEN by exchange factor P-REX2a. *Science*. 2009;325(5945):1261–1265.
38. Uhlenhaut NH, et al. Insights into negative regulation by the glucocorticoid receptor from genome-wide profiling of inflammatory cistromes. *Mol Cell*. 2012;49(1):158–171.
39. Chinenov Y, Sacta MA, Cruz AR, Rogatsky I. GRIP1-associated SET-domain methyltransferase in glucocorticoid receptor target gene expression. *Proc Natl Acad Sci U S A*. 2008;105(51):20185–20190.
40. Wu SP, Lee DK, Demayo FJ, Tsai SY, Tsai MJ. Generation of ES cells for conditional expression of nuclear receptors and coregulators in vivo. *Mol Endocrinol*. 2010;24(6):1297–1304.
41. Park JH, et al. Prostatic intraepithelial neoplasia in genetically engineered mice. *Am J Pathol*. 2002;161(2):727–735.
42. Xie X, Qin J, Lin SH, Tsai SY, Tsai MJ. Nuclear receptor chicken ovalbumin upstream promoter-transcription factor II (COUP-TFII) modulates mesenchymal cell commitment and differentiation. *Proc Natl Acad Sci U S A*. 2011;108(36):14843–14848.
43. Qin J, Chen X, Xie X, Tsai MJ, Tsai SY. COUP-TFII regulates tumor growth and metastasis by modulating tumor angiogenesis. *Proc Natl Acad Sci U S A*. 2010;107(8):3687–3692.
44. Cancer Genome Atlas Research Network.

Comprehensive molecular characterization of clear cell renal cell carcinoma. *Nature*. 2013;499(7456):43–49.
45. Creighton CJ, et al. Integrated analyses of microRNAs demonstrate their widespread influence on gene expression in high-grade serous ovarian carcinoma. *PLoS One*. 2012;7(3):e34546.
46. Cancer Genome Atlas Research Network. Integrated genomic analyses of ovarian carcinoma. *Nature*. 2011;474(7353):609–615.
47. Luo J, et al. A genome-wide RNAi screen identifies multiple synthetic lethal interactions with the Ras oncogene. *Cell*. 2009;137(5):835–848.
48. Creighton CJ, et al. Residual breast cancers after conventional therapy display mesenchymal as well as tumor-initiating features. *Proc Natl Acad Sci U S A*. 2009;106(33):13820–13825.
49. Creighton CJ, et al. Insulin-like growth factor-I activates gene transcription programs strongly associated with poor breast cancer prognosis. *J Clin Oncol*. 2008;26(25):4078–4085.
50. Cancer Genome Atlas Research Network. Integrated genomic analyses of ovarian carcinoma. *Nature*. 2011;474(7353):609–615.